Accepted Manuscript

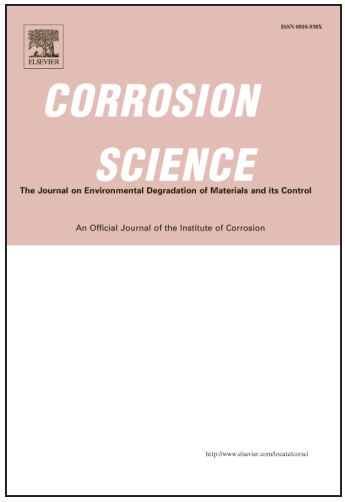

Corrosion mechanism and evaluation of anodized magnesium alloys

Guang-Ling Song, Zhiming Shi

PII: S0010-938X(14)00168-1
DOI: http://dx.doi.org/10.1016/j.corsci.2014.04.008
Reference: CS 5802

To appear in: *Corrosion Science*

Received Date: 15 October 2013
Accepted Date: 7 April 2014

Please cite this article as: G-L. Song, Z. Shi, Corrosion mechanism and evaluation of anodized magnesium alloys, *Corrosion Science* (2014), doi: http://dx.doi.org/10.1016/j.corsci.2014.04.008

CORROSION MECHANISM AND EVALUATION OF ANODIZED MAGNESIUM ALLOYS

Guang-Ling Song*, Zhiming Shi

The University of Queensland, Materials Engineering,
St Lucia, Brisbane, Qld 4072, Australia,
*Current correspondence: Materials Science and Technology Division, ORNL National Lab,
1 Bethel Valley Rd, Oak Ridge, TN37831, USA
guangling.song@gmail.com

Abstract:

The corrosion of anodized Mg alloys is investigated by means of immersion, salt spray, polarization curve, AC electrochemical impedance spectroscopy (EIS), SEM and optical microscopy analyses. Based on the blocking, retarding and passivating effects of an anodized coating on corrosion of Mg alloys, a corrosion model is proposed to illustrate the corrosion reaction at the coating/substrate interface in coating through-pores. It is found that EIS can sensitively respond to the occurrence of corrosion in anodized Mg alloys and reflect the protection performance of anodized coatings, which may be used as an in-situ method of monitoring corrosion for anodized Mg alloys.

Keywords: Magnesium, Anodizing, Corrosion, EIS, Polarization

1. Introduction

Magnesium alloys as structural materials are attractive to the automotive, aerospace and electronic industries for their low density, high ratio of strength to weight, excellent castability and good electromagnetic interference shielding property [1-3]. Mg alloys are also great functional materials and could be used as battery electrodes, sacrificial anodes, hydrogen storage materials and even biodegradable implants [**Error! Bookmark not defined.**]. Unfortunately, these fascinating properties are offset by their highly reactive nature or low corrosion resistance [8-12]. Currently, Mg alloys in the automotive industry are simply being considered for uses in mild service environments [13-15]. Significantly improving the corrosion resistance of Mg alloys is a challenging task.

A variety of surface treatments have been proposed to protect Mg alloys from corrosion. Anodizing is one of the most popular processes [16]. Mg anodizing in many cases is also known as a micro-arcing process due to the eye-catching sparking phenomenon in the bath. However, in nature it is still an anodizing reaction between Mg substrate and the bath electrolyte. Several commercial coatings have been developed for Mg alloys, such as Tagnite [17], Anomag [18], Magoxid [19], Keronite [20], HAE [21] and Dow 17 [22], and numerous new anodizing techniques are being proposed [23-25]. Current anodizing studies range from coating formation mechanisms to post-treatments [26-30]. Having realized some limitations of existing anodizing techniques, researchers recently have started to explore composited coating systems that include an anodized layer as the base and another film as its top [31]. For example, Song et al [32-34] developed a rapid

dipping electroless E-coating process which can be applied to anodized Mg alloys to significantly improve their corrosion performance [35-37].

Normally, anodized coatings on Mg alloys are porous [**Error! Bookmark not defined.**,38,39]. The core technique of anodizing includes control of baths and optimization of operation conditions in order to form a uniform, stable and less porous oxide layer on Mg alloys. The thickness, stability and porosity of an anodized coating can influence the protection performance of an anodized coating, and these coating parameters are also functions of substrate phase constituent and microstructure, electrolyte composition and concentration, anodizing current density and voltage. Therefore, the corrosion resistance of an anodized Mg alloy is eventually determined by the substrate, bath and operation parameters, all of which should be carefully selected and controlled in practice [40-45].

Almost all the developed anodized coatings are claimed by their inventors to be able to satisfactorily protect Mg alloy components from corrosion attack. It is important to know which anodizing process is really suitable for a given Mg alloy component in the service environment. A normal way of assessing and comparing anodized Mg alloys is the well-known salt spray test [**Error! Bookmark not defined.**, 46]. However, this method is time-consuming and does not provide detailed information on corrosion mechanism. There is a need for a rapid informative method to evaluate anodized Mg alloys in the auto industry, particularly when there are a large number of anodized samples. Such a method is also essential for gaining a deep insight into the corrosion mechanism of anodized Mg

alloys and understanding the corrosion behavior of anodized coatings. Establishment of such a technique may provide a solid foundation for developing more robust coatings for Mg alloys.

Since electrochemical reactions are responsible for corrosion damage, electrochemical techniques should be capable of revealing the corrosion mechanism and evaluating the corrosion performance of anodized Mg alloys. There are hundreds of publications using EIS in Mg corrosion studies, but most of them are on bare Mg alloys [47,48], and some on conversion and organic coatings [49-52]. Not many EIS studies are on anodized Mg alloys. In the limited number of EIS investigations of anodized Mg alloys, the AC impedance features, such as capacitive and inductive loops, are mainly employed to characterize the overall corrosion resistance of anodized coatings [53-55]; their physical meanings are not very clear or have not been convincingly interpreted [56]. Some researchers employed existing equivalent circuits from other systems to explain the corrosion of anodized coatings [57] or proposed new equivalent circuits with clear physical meanings for all the circuit components to analyze their EIS results [58]. However, they failed to justify theoretical foundations for the selected or proposed EIS models. For example, it is unclear why the equivalent components must be in series not parallel, or why the circuit should evolve or change with time in that way [59-61].

Although in the equivalent circuits used by Yagi *et al.* [**Error! Bookmark not defined.**], elements representing coating pores have been included, the electrochemical processes in these pores have not been explored further. In fact, defects, like pores and micro-cracks, are critical sites that determine the protection performance of an anodized coating. The

electrochemical processes in these defects contain a wealth of useful information on coating degradation. A detailed EIS model that can illustrate the corrosion reaction inside the defects of an anodized coating will undoubtedly be helpful in understanding the corrosion mechanism and evaluating the corrosion performance of anodized Mg alloys. Unfortunately, pertinent studies on so detailed corrosion mechanism of anodized coatings on Mg alloys are still relatively rare currently.

This paper will employ polarization curve and AC impedance techniques together with Scanning Electron Microscope (SEM) to investigate the corrosion behavior of anodized Mg alloys, aiming to establish a comprehensive EIS model to understand their corrosion mechanisms and also to obtain a rapid non-destructive method for evaluating and monitoring the protection performance of anodized coatings on Mg alloys.

2. Experimental Details

If not specified, all the tests were conducted at ambient temperature and the solutions used in the study were prepared using analytical purity chemicals and demineralized water. All the potentials are relative to an Ag/AgCl reference electrode if not specified in the following text or denoted in figures.

2.1. Alloys, specimens and testing solutions

Magnesium alloys AZ91D (8.3-9.7 wt.% Al, 0.35-1 wt.% Zn, 0.15-0.50 wt.% Mn), ZE41 (3.5-5 wt.% Zn, 0.4-1.0 wt.% Zr, 0.75-1.75 wt.% rare earth elements) and pure Mg (99.96 wt.%) were cut from ingots, machined into coupons (2cm × 2cm × 0.5cm), abraded to P#1200 with SiC paper, degreased with ethanol and then dried in air. These specimens were stored in a desiccator in the lab before experiments.

Various amounts of NaCl were mixed with $Mg(OH)_2$ in demineralized water to make up $Mg(OH)_2$-saturated NaCl solutions, which contained 0.1 wt.% NaCl, 0.5 wt.% NaCl and 5 wt.% NaCl, respectively. Their pH values were ~11 because of saturated $Mg(OH)_2$. They were used in AC impedance and polarization measurements as electrochemical test solutions in this study. Another solution, 5 wt.% NaCl (pH~7) without $Mg(OH)_2$, was also prepared and used as a corrosion test solution in immersion and salt spray experiments.

2.2. Anodizing

The samples were anodized using a KSP process that has been reported in literature [**Error! Bookmark not defined.**]. The samples were immersed in an alkaline solution containing borate and silicate (12 wt.% NaOH + 12 wt.% $Na_4B_2O_7.10H_2O$ + 9 wt.% Na_2SiO_3) at 75-95 °C to remove surface oil and contaminants. After being washed with demineralized water and dried, they were anodized in an alkaline electrolyte containing silicate and potassium hydroxide (1.6 wt. % K_2SiO_3 + 1 wt.% KOH) at ambient temperature. The anodizing current density was controlled at 20 mA/cm^2 for 10 minutes,

then 10 mA/cm^2 for 10 minutes and finally 5mA/cm^2 for 10 minutes. The anodized specimens were then washed with demineralized water and dried in air.

For comparison purposes, some ZE41 specimens were anodized using a commercial anodizing process Tagnite™. A few Anomag™ anodized AZ91D die-casting plates (8cm × 12cm × 0.3cm) that had been exposed to 5 wt.% NaCl salt spray for 21 days were also used in this study.

2.3. Potentiodynamic polarization and AC electrochemical impedance

Polarization curve and AC electrochemical impedance spectroscopy (EIS) measurements were conducted using a three-electrode flat electrolyte cell system (Princeton Applied Research, K0235) which has a 1 cm^2 open window for a working electrode to expose its flat surface to the electrolyte in the cell. The working electrode specimen in a slot holder outside the cell was attached tightly to the window by a steel screw bolt through the holder. The bolt pushed the specimen firmly against the window, and also acted as an electrical conductor to connect the working electrode specimen to an electrochemical measurement system (Solatron 1260). Anodized and unanodized coupons in normal size (2cm × 2cm × 0.5cm) were directly placed in the electrode holder and attached to the cell open window. Those larger samples, like Anomag and Tagnite anodized die-casting plates (8cm × 12cm × 0.3cm), were cut into smaller coupons (3cm × 3cm × 0.3cm) before being attached to the window. A KCl saturated (4.2 mol./L KCl) Ag/AgCl electrode, which is 0.197 V more positive than the standard hydrogen electrode in equilibrium potential, was used as reference in the cell, and the auxiliary electrode was a

platinum mesh. The electrolyte cell contained 450 mL of $Mg(OH)_2$ saturated 0.1 wt.% NaCl solution. The specimen was immersed in the solution for 0.5 hour to allow its corrosion potential or corrosion potential (E_{corr}) to reach a relatively stable value. As EIS measurement does not significantly alter the corrosion status of an electrode system, it was carried out first on the specimen at its corrosion potential E_{corr}. A 10 mV peak-to-peak amplitude of AC potential signal was selected. Frequency range was from 100 kHz to 10 mHz. On completion of EIS measurement, polarization curve measurement was carried out immediately. Potentiodynamic scanning rate was set at 0.167 mV/s. Under each testing condition, AC impedance and polarization curve measurements were repeated 3~7 times, depending on experiment reproducibility. If an experiment had good reproducibility, it was simply repeated 3 times. In case of bad reproducibility, 7 repetitions were required for the same measurement.

2.4. Immersion and salt spray

Anodized specimens were immersed in 5 wt.% NaCl solution in beakers, and their corrosion morphologies after immersion were recorded. The corrosion rates of unanodized specimens after immersion in the same corrosion test solution were estimated through weight loss measurement. The corrosion products on the unanodized specimens were removed by dipping the corroded samples in solution 200g/L CrO_3 +10g/L $AgNO_3$ for several minutes until no further gas bubbles came out from the surfaces. They were then washed with demineralized water, dried and weighed for their weight loss. At least 3 parallel immersion tests were performed to obtain an average weight loss rate for each

sample. The effect of CrO_3+$AgNO_3$ cleaning on the mass change of Mg and its alloys has been carefully investigated [62-64]. It is concluded that the chromic acid cleaning will not significantly remove metallic Mg or cause evident deposition of chromic products on the metal surface. In this study, after weight loss measurements, no subsequent tests were conducted on the chromic acid cleaned samples. Therefore, there wouldn't be any possible interference of deposited chromium oxides with other experiments.

Salt Spray Test (SST) of anodized specimens was conducted according to ASTM B117 [**Error! Bookmark not defined.**] in a Vötsch Industrietechnik VSC 450 chamber using 5 wt.% NaCl corrosion test solution. The chamber temperature was controlled at 35°C and the pH value of the salt solution was around 7.0. KSP anodized and Tagnite anodized ZE41 specimens were exposed in the fogy chamber for 3 days and 12 days, respectively. Anomag anodized AZ91D was exposed for 21 days.

2.5. SEM and optical microscopy

The microstructures of anodized specimens were examined under a JEOL 6460 scanning electronic microscope. To reveal the corrosion penetration in an anodized coating, Anomag and Tagnite anodized ZE41 samples after immersion were also cross-sectioned along corroded areas and observed under an optical microscope.

3. Results

3.1. Immersion corrosion of anodized and unanodized Mg alloys

Figure 1 shows the corrosion damage morphologies of Mg alloys after immersion. The KSP anodized Mg was severely corroded after only 1 day immersion (see Figure 1(a)). In the lab, the corrosion penetration deep into the KSP anodized Mg substrate in a few areas can actually be easily visualized by naked eye. The corrosion of KSP anodized ZE41 (see Figure 1(c)) spread out widely after 2 days in the same corrosion test solution. Naked-eye examination in the lab confirmed that the corrosion did not penetrate deeply into ZE41. On KSP anodized AZ91D, minor pitting damage was visualized after 11 days of immersion (see Figure 1(b)). From these damage morphologies, it can be concluded that KSP anodized AZ91D is better than KSP anodized ZE41, and KSP anodized Mg is the least corrosion resistant. Their corrosion resistance can be ranked in the order: AZ91D>ZE41>Mg.

The weight loss rates of unanodized Mg, ZE41 and AZ91D after immersion in the same corrosion test solution are listed in Table 1. Their clearly different corrosion rates after 6 hours of immersion are evident enough to demonstrate that their corrosion resistances have the following order: Mg<ZE41<AZ91D.

Table 1. Weight loss rates and standard deviations of Mg, ZE41 and AZ91D after immersion in 5 wt.% NaCl for 6 hours

Specimen	Mg	ZE41	AZ91D
Weight loss rate, mg/cm^2/hour	0.52	0.20	0.05
(Standard deviation)	(0.10)	(0.10)	(0.04)

3.2. Salt spray corrosion performance of anodized ZE41

The corrosion morphologies of KSP and Tagnite anodized ZE41 after exposure in 5 wt.% NaCl salt spray are shown in Figure 2. The Tagnite anodized ZE41 (see Figure 2(b)) is better than the KSP anodized (see Figure 2 (a)). The corrosion damage area on the former after 12 days of exposure is still much smaller than that of the latter which has only been exposed for 3 days. This suggests that the Tagnite anodized ZE41 is more corrosion resistant than the KSP.

3.3. Polarization curves

The polarization curves for ZE41 in 5 wt.% NaCl solutions saturated and not saturated with $Mg(OH)_2$, respectively, are shown in Figure 3. The polarization curves in the 5 wt.% NaCl solution are relatively scattered, particularly the anodic branches (Figure 3(a)). The addition of $Mg(OH)_2$ improves the polarization curve reproducibility, because all the measured polarization curves become almost overlapped in the $Mg(OH)_2$ saturated 5 wt.% NaCl solution (Figure 3(b)).

Figure 4 presents the polarization curves of ZE41 alloy in $Mg(OH)_2$ saturated NaCl solutions with different concentrations of chloride. It shows that reducing chloride concentration leads to a decrease in anodic current density or passive current density (I_p) and an increase in pitting potential (E_{pt}). The anodic polarization curve obtained in the $Mg(OH)_2$ saturated 0.1 wt.% NaCl solution has a more evident pitting potential and passive region than those in the solutions containing higher concentrations of chloride. The polarization curve for KSP anodized ZE41 in $Mg(OH)_2$ saturated 0.1 wt.% NaCl solution is also displayed in Figure 4. The KSP anodizing leads to an increased pitting potential (E_{pt}) and a significantly decreased passive current density (I_p).

The typical anodic polarization curves for KSP anodized Mg, ZE41 and AZ91D and Tagnite anodized ZE41 in $Mg(OH)_2$ saturated 0.1 wt.% NaCl solution are shown in Figure 5. Different substrates and anodizing treatments result in some differences in polarization behavior. The average values of E_{pt} and I_p obtained from repeatedly measured polarization curves are listed in Table 2. The KSP anodized AZ91D has the lowest I_p, while I_p of KSP anodized Mg is much higher than that of the KSP anodized ZE41. The E_{pt} of KSP anodized Mg is slightly more negative than that of KSP anodized ZE41, but it is more positive than that of anodized AZ91D. The Tagnite anodized ZE41 has an even lower I_p and more positive E_{pt} than KSP anodized ZE41, AZ91D and Mg.

Table 2. Average values and standard deviations of the electrochemical parameters of KSP anodized Mg, AZ91D and ZE41 and Tagnite anodized ZE41 after immersion in $Mg(OH)_2$ saturated 0.1 wt.% NaCl solution for 0.5 hour

	E_{corr} (V, Ag/AgCl/Sat.KCl)	Std. dev.	R_1 (Ω·cm^2)	Std. dev.	E_{pt} (V, Ag/AgCl/Sat.KCl)	Std. dev.	I_p (A/cm^2)	Std. dev.
KSP Mg	-1.71	0.04	1.8×10^{5}	5.5×10^{4}	-1.06	0.04	4.7×10^{-6}	2.2×10^{-7}
KSP AZ91D	-1.35	0.05	9.5×10^{6}	3.4×10^{6}	-1.17	0.07	2.1×10^{-7}	2.4×10^{-8}
KSP ZE41	-1.39	0.09	2.1×10^{6}	7.5×10^{5}	-1.08	0.12	3.8×10^{-6}	8.3×10^{-7}
Tagnite ZE41	-1.45	0.04	3.3×10^{7}	1.3×10^{7}	-0.87	0.11	3.0×10^{-7}	4.4×10^{-8}

3.4. AC electrochemical impedance spectrum (EIS)

Unanodized ZE41 in $Mg(OH)_2$ saturated 0.1 wt.% NaCl solution has an AC electrochemical impedance spectrum (EIS) containing two capacitive loops in the high and mediate frequency ranges and an inductive loop in the low frequency range (see Figure 6 (a)). The typical EISs of KSP anodized Mg, ZE41 and AZ91D after immersion in $Mg(OH)_2$ saturated 0.1wt.% NaCl for 0.5 hour (see Figure 6 (b), (c) and (d)) also appear to have two capacitive loops in the high and mediate frequency ranges and some inductive characteristics in the low frequency range, but the mediate frequency capacitive loop is much larger than the high frequency one; in some cases, these two capacitive loops are completely merged together and difficult to distinguish (e.g. Figure 6(b)); sometimes the low frequency inductive loop even disappears (e.g. Figure 6(d)).

The overall capacitive loop diameter, i.e., the sum of diameters of the high and mediate frequency semicircles, is denoted as R_1. For simplicity, the capacitive loops in the high and mediate frequency ranges can be treated as a large semicircle, and thus a simple $R_1//Q_1$ equivalent circuit (Q_1 is a constant phase component representing a non-ideal capacitance) can be employed to estimate the overall capacitive loop diameter R_1. As the

high frequency loop is much smaller than the mediate frequency semicircle, this simplification will not introduce a significant error to the R_1 value. The average values of R_1 for KSP anodized specimens at the beginning of immersion are listed in Table 2. Meanwhile, the corrosion potentials (E_{corr}) measured before EIS experiments are also listed there. The estimated R_1 values for KSP anodized ZE41, AZ91D and Mg can be ranked in the following order: AZ91> ZE41 > Mg. It is a reversed order of I_p (see Table 2).

Figure 7 shows the EISs changing with time for KSP and Tagnite anodized ZE41 immersed in the $Mg(OH)_2$ saturated 0.1 wt.% NaCl solution. At beginning, the EISs appear to have two capacitive loops and the second one is too large to be completely measured; no inductive characteristic can be detected in the low frequency range. With time, the capacitive loops gradually become smaller. After a certain period of time, inductive characteristics emerge in the low frequency range, and the two capacitive loops in the high and mediate frequency ranges are merged together, becoming one loop. In this case, although the capacitive diameters have already become significantly smaller than that at the beginning of immersion, the corrosion damage on the coatings may not be visible by naked eye. Normally, only after R_1 is below the order of $k\Omega \cdot cm^2$, can corrosion damage be clearly seen on these coatings.

To better illustrate the relationship between corrosion damage and EIS behavior, Anomag anodized die-cast AZ91D plates that had been exposed in salt spray (ASTM-B117) for 21 days were also tested. EISs were measured on two selected surface areas of the plates:

one has significant corrosion damage and on the other one the damage is insignificant (at least cannot be easily detected by naked eye). Figure 8 shows the EISs obtained from these two areas. Their EIS spectra are similar; both have a large capacitive semicircle and a small inductive loop, but their diameters are very different; the capacitive and inductive loops for the area not significantly corroded are over two orders of magnitude larger than those for the significantly corroded areas.

3.5. Microstructure

The topographic SEM images of KSP, Tagnite and Anomag anodized coatings on pure Mg, AZ91D and ZE41 are shown in Figure 9. All the coatings are porous. The pore size is in the range of 1~3 micrometer (see the roughly measured pore size listed in Figure 9). Compared with the microstructures of KSP anodized coatings on Mg, AZ91 and ZE41 (see Figure 9 (a), (b) and (c)), Tagnite and Anomag coatings on ZE41 (Figure 9 (d) and (e)) also have many randomly distributed pores, but their porosity appears to be slightly lower than that of KSP coatings. The cross-sectional SEM images of KSP, Tagnite and Anomag anodized ZE41, together with their pore sizes, are presented in Figure 10, which further illustrate pores throughout the coatings. The images show that Tagnite coating is thicker than SKP and Anomag in this study. The pore diameters roughly measured from the cross-section images appear to be different from those obtained from the topographic photos. This is due to the complicated pore shape and non-uniform pore distribution in the coatings.

Anomag anodized ZE41 after 20 hour immersion in $Mg(OH)_2$ saturated 0.1NaCl solution and Tagnite anodized ZE41 after 12 day exposure in 5 wt.% NaCl fog were cross-sectioned and examined under a light microscope. The uncorroded region of Anomag coating and corroded area of Tagnite coating are shown in Figure 11. The Anomag coating is relatively thin and not very uniformly formed (see Figure 11 (a)); corrosion penetrates deeper into the substrate along the grain boundaries (as indicated by the short arrows in the photo); some corrosion damage in the substrate is also observed under a coating pore in grain central area as pointed by the long arrow in the photo (Figure 11 (a)). For Tagnite coating on ZE41, no corrosion damage can be observed under the coating in the uncorroded area. In corroded area, corrosion penetrates deeply into the substrate ZE41 and loose corrosion products form there. Figure 11 (b) shows that undermining of substrate (as indicated by the arrow) occurs, developing from the corroded region into the substrate under the uncorroded coating.

4. Discussion

4.1. Coating model and corrosion mechanism

1) Coating effect

Published research [**Error! Bookmark not defined.**,**Error! Bookmark not defined.**,**Error! Bookmark not defined.Error! Bookmark not defined.**] and the microstructure analyses (Figure 9 and Figure 10) in this study have clearly shown that the anodized coatings are porous. Due to the porosity, corrosive solution can get into an

anodized coating and reach the substrate after a certain period of time. Nevertheless, an anodized coating can still to some extent retard the ingress of corrosive species and significantly delay the corrosion of anodized Mg alloys. The role of an anodized coating slowing down the ingress of corrosive species in corrosion is termed "retarding effect" in this paper.

In an anodized coating, most pores are randomly and separately distributed in the coating layer (see Figure 10); only a small number of them can penetrate through the coating from the outmost surface to the substrate. This kind of pore is defined as "through-pore" in this paper. Only the through-pore can act as a corrosion "short-cut" in an anodized coating; "non-through-pore" does not have a direct contribution to the corrosion of an anodized Mg alloy. Thus, the protection performance of an anodized coating cannot be predicted simply based on coating porosity or pore size that mainly characterizes the non-through pores. In the event that corrosive solution finally reaches the coating/substrate interface in the through-pores, the area of the substrate directly exposed to the solution is actually very limited. Therefore, an anodized coating can effectively restrict the area of a Mg alloy in contact with the environmental solution. This limitation is named "blocking effect" in this paper.

An anodized coating can also passivate substrate defects or active points that are susceptible to corrosion attack. These sites can be grain boundaries or impurity particles. After anodizing, these active points are still preferentially subjected to corrosion attack when corrosive solution penetrates through the coating [**Error! Bookmark not defined.**].

Figure 11 (a) shows an example for such corrosion damage of anodized Mg alloys; the pores in the coating above the substrate defective zones (e.g. grain boundaries) provide short-cuts for corrosive solution to attack the substrate. Fortunately, the probability is not high that a through-pore in the coating happens to be right over the substrate defective/active point, particularly when the anodized coating is relatively thick and compact. In other words, it is unlikely for an active or defective site to be directly exposed to corrosive solution under a through-pore. In most cases, a "passive" area of the substrate is under the through-pore. By concealing defective/active points, an anodized coating can significantly improve the corrosion resistance of a Mg alloy. This is a "passivating" effect of an anodized coating on the substrate Mg alloy.

In theory, it would be ideal if the "retarding", "blocking" and "passivating" effects could be separately identified and their beneficial contributions to the protection performance of an anodized coating be quantitatively estimated, respectively. However, in reality it is very challenging, as the three different mechanisms usually operate together. When aggressive electrolyte has got into a coating and starts to attack the substrate in a through-pore, the substrate passivity will become an important factor in determining the corrosion process. Meanwhile, the penetrated or broken coating can still to a great degree slow down the supply of corrosive species and the removal of corrosion products. In the same time, the undamaged coating area can still effectively stop the corrosion of the substrate from spreading. More complicatedly, the three effects can interact with one another during corrosion. While an anodized coating degrades and the coating retarding effect becomes less significant, the blocking effect also decreases, which leads to deteriorated

substrate passivity. To separately investigate the three individual effects on corrosion of anodized Mg alloys, many systematically designed experiments with carefully prepared anodized coatings are needed. Such a comprehensive study cannot be covered in this paper. Fortunately, without distinguishing these three effects, one can still develop a deeper understanding of the corrosion mechanism of anodized Mg alloys, which will be demonstrated later in this paper.

2) Corrosion process

It should be noted that on Mg and its alloys, there is always a spontaneously/naturally formed surface film mainly consisting of MgO and $Mg(OH)_2$ [**Error! Bookmark not defined.**]. This film is much thinner than an anodized coating. Corrosion of the substrate can easily occur in the film-free areas [**Error! Bookmark not defined.**,**Error! Bookmark not defined.**]. After anodization, such a spontaneously formed surface film could still be on the substrate surface in coating through-pores. When an anodized specimen is immersed in a corrosive solution, the solution including aggressive ions (e.g. Cl^- cations) will get into through-pores and eventually reach the substrate/coating interface, where the solution will be in contact with the bare substrate surface in the film-free areas. After the concentration of Cl^- increases above a critical threshold (supposed to be much lower than 5 wt.%), the substrate Mg is rapidly dissolved into the pore solution in the through-pores from the film-free areas of the substrate, which will make the pore solution saturated with $Mg(OH)_2$. Hence, the substrate Mg alloy surface is actually exposed to a $Mg(OH)_2$ saturated NaCl solution in the coating through-pores, and the

corrosion of an anodized Mg alloy is in effect a reaction between the substrate Mg alloy and a $Mg(OH)_2$ saturated NaCl solution.

Based on the above corrosion process description, the corrosion of an anodized Mg alloy can be schematically illustrated in Figure 12. The naturally/spontaneously formed porous surface film (Figure 12 (a)) is a discontinuous layer, and the film-free areas can be treated as kinds of film through-pores like those in anodized coatings. After anodizing, in a through-pore of an anodized coating, the porous surface film is still on the substrate as shown in Figure 12 (b); in the illustration (Figure 12 (b)), a grain boundary is exaggeratedly arranged right under a coating through-pore as a defective/active site. Corrosion initiates from the defective/active site of the substrate exposed to the solution in a through-pore (Figure 12(c)). After corrosion, loose corrosion products are deposited in the coating damaged or corroded area, which are not illustrated in Figure 12 (d).

Figure 10 and Figure 11 (a) and (b) provide experimental evidence for the corrosion process of an anodized Mg alloy at beginning, during corrosion initiation and after corrosion damage, respectively as described in the model (Figure 12 (a), (b) and (c)). Although the coating is highly porous, the number of through-pores is not large (Figure 10). Corrosion does initiate under a through-pore (see the long arrow in Figure 11 (a)). After coating breakdown, severe corrosion can occur in the substrate (Figure 11 (b)). The proposed corrosion mechanism (Figure 12) will be further verified as follows.

4.2. Electrochemical verification

1) Polarization behavior

The polarization behavior of anodized ZE41 in $Mg(OH)_2$ saturated 0.1 wt.% NaCl solution (see Figure 4) can be easily understood based on the proposed coating effects and corrosion model (Figure 12). The anodic polarization current of anodized ZE41 represents Mg dissolution rate in coating through-pores. The decreased passive current density and increased pitting potential after anodizing compared with those of unanodized ZE41 can be ascribed to the blocking and passivating effects of the coating. The blocking effect limits anodic dissolution current, and the passivating effect also leads to a decreased current density. Substrate defective sites have relatively negative corrosion and pitting potentials. After covered by an anodized coating, the corrosion and pitting potentials certainly become more positive.

2) AC impedance behavior

According to the proposed corrosion process (Figure 12) and coating effects, the EIS behaviors of anodized specimens (Figure 6, Figure 7 and Figure 8) can be predicted.

Unanodized ZE41 (Figure 6 (a)) has some EIS characteristics similar to pure Mg and AZ91D in a NaCl solution reported before [66,67]. According to Song *et al.*'s electrochemical interpretation [**Error! Bookmark not defined.**,**Error! Bookmark not defined.**], the dissolved Mg^+ and surface film are responsible for the mediate frequency capacitive and low frequency inductive behaviors, while the first capacitive loop in the high frequency range can be ascribed to a charge transfer resistance R_t and a capacitance $C_{s/m}$ between solution and Mg substrate. The similarity of the unanodized ZE41 to the reported Mg [**Error! Bookmark not defined.**] and AZ91D [**Error! Bookmark not defined.**] in EIS suggests that ZE41 has the same corrosion mechanism as Mg and AZ91D: ZE41 has a spontaneously/naturally formed thin porous film; Mg is oxidized into Mg^+ and dissolved into solution in the film-free area; the film-free area enlarges when applied potential increases.

According to the proposed corrosion model (Figure 12), on anodized ZE41 with a porous coating (Figure 9 and Figure 10), the electrochemical reactions at the coating/substrate interface in a through-pore should be the same as those on unanodized ZE41, but their rates are significantly lower due to the retarding, blocking and passivating effects of the anodized coating. The corrosion in such an anodized system can be depicted by an equivalent circuit as shown in Figure 13. In the circuit, each component has a clear physical meaning: R_s stands for the solution resistance between reference electrode and specimen; $C_{s/m}$ is the capacitance between the solution and Mg substrate, which is equal to capacitance of the anodized coating; $R_{coating}$ denotes the anodized coating resistance which is determined by the coating thickness and porosity, particularly the number of

through-pores; R_t represents the charge transfer resistance at the coating/substrate interface in through-pores; C_{Mg+} and R_{Mg+} symbolize pseudo capacitance and resistance caused by the involvement of Mg^+ in Mg dissolution [**Error! Bookmark not defined.**]; R_f and L_f are also pseudo resistance and inductance resulting from breakdown of the substrate surface film in through pores or the anodized coating by increasing potential [**Error! Bookmark not defined.**].

The construction of this equivalent circuit or connection of components in the circuit (Figure 12) is based on the following mechanistic consideration: A steady electrochemical reaction more complicated than a simple one step metal-solution transfer procedure can be equivalent to a charge transfer resistance connecting in series with a pseudo resistance and a pseudo capacitance; the latter two are connected in parallel. Thus, the components R_{Mg+} representing the Mg^+ involved dissolution reaction at the coating/substrate interface should have a circuit connection like R_t (C_{Mg+}//R_{Mg+}), which normally has a capacitive loop in the mediate frequency range on Nyquist plot. The breakdown of the film on the substrate as well as the anodized coating also initiates at the coating/substrate interface in coating through-pores. On Nyquist plane, it normally exhibits some inductive characteristics at low frequencies, and its equivalent components are R_f and L_f in series. As the film breakdown occurs in parallel with the Mg^+ involved dissolution, there is (R_f L_f)//(R_t (C_{Mg+}//R_{Mg+})). The through-pores can be treated as paths to these two parallel electrochemical reactions at the coating/substrate interface. Since $R_{coating}$ is mainly determined by the conductivity of through-pores, it can be connected to the above circuit in series: $R_{coating}$((R_f L_f)//(R_t (C_{Mg+}//R_{Mg+})). Obviously, the $C_{s/m}$

representing the capacitance across the anodized coating from solution to substrate is a parallel component connecting with the above circuit: $C_{s/m}(R_{coating}\ (R_f\ L_f)//(R_t\ (C_{Mg+}//R_{Mg+})))$. After the solution resistance R_s is introduced, an equivalent circuit is yielded as shown in (Figure 12), which clearly demonstrates the relationship of difference reactions and processes involved in the anodized coating during corrosion.

As predicted by this equivalent circuit (Figure 13), an anodized Mg system should have 3 time-constants: two capacitive loops in the high and mediate frequency ranges and an inductive loop in the low frequency. The experimentally measured EISs (Figure 6, Figure 7 and Figure 8) have more or less demonstrated the modelled EIS behaviors.

The reasonability of the equivalent circuit (Figure 13) can be verified by regressing it into a simple one for an unanodized Mg. Let $R_{coating}$=0, the equivalent circuit will describe an unanodized Mg alloy. It gives out an EIS spectrum that still contains two capacitive loops in the high and mediate frequency ranges and an inductive loop in the low frequency range (see Figure 14 (a)), which matches the measured EIS of unanodized ZE41 (Figure 6(a)).

When a thick anodized coating is formed, $R_{coating}$ will have a large value. Due to the existence of this coating between substrate and solution, $C_{s/m}$ becomes much smaller. Meanwhile, as only a tiny surface area of the substrate and a very small number of defective/active sites are exposed to the solution in coating through-pores, R_t becomes

considerably larger. Certainly, the other equivalent components C_{Mg+}, R_{Mg+}, R_f and L_f for the anodized specimen will also have values different from those of its unanodized counterpart. At the beginning of immersion when solution has not reached the substrate and corrosion at the coating/substrate has not been initiated, no R_{Mg+}, C_{Mg+}, L_f or R_f needs to be considered. The equivalent circuit can be simplified by setting $C_{Mg+} = \infty$, $R_{Mg+} = 0$, $L_f = \infty$, and $R_f = \infty$. Consequently, an EIS with a single capacitive semicircle as shown in Figure 14(b) will be obtained. It has the same capacitive characteristics as the initial Tagnite EISs (Figure 7 (b)).

After the environmental solution gets into the coating through-pores, $R_{coating}$ will be significantly reduced. Before Cl^- increases above the critical threshold in the pores, it cannot significantly damage the anodized coating or the surface film of the substrate in coating through-pores, but Mg dissolution can be accelerated in the film-free area of the substrate in coating through-pores. Thus, R_t becomes smaller. In this case, R_{Mg+} and C_{Mg+} must be considered and should be included in the equivalent circuit. As the reactions at the coating/substrate interface in the coating through pores in this stage are stilly slow and the involvement of Mg^+ is not significant, R_{Mg+} may have a relatively large value and C_{Mg+} could still be very small. Thereby, the model-predicted EIS will have 2 capacitive loops like those in Figure 14(c), which explains the experimental EIS behaviors of KSP anodized ZE41 and AZ91D (Figure 6(c) and (d) and Figure 7(a)) in the initial stage of immersion. The experimentally measured EISs without inductive characteristic in the first few hours of immersion as shown in Figure 6(c) and (d) and

Figure 7 imply that the KSP and Tagnite coatings on AZ91D and ZE41 have not been damaged by Cl^- in this stage.

With immersion time, the increased concentration of Cl^- in coating through-pores will eventually cause damage to the substrate film and the anodized coating. The film or coating damage related components L_f and R_f in the equivalent circuit (Figure 13) will not be infinite anymore in this case. They will generate an inductive loop at low frequencies (see Figure 14(d)). The film and coating damage will also significantly reduce the coating resistance and make Mg (involving Mg^+) dissolution easier, i.e., $R_{coating}$ and R_{Mg+} become smaller. Thus, the capacitive loops at high and mediated frequencies shrink while the inductive characteristic is emerging. The EIS evolution behaviors (Figure 7) of KSP and Tagnite coatings on ZE41 experimentally prove such a process. In practice, it is possible that the coating-related high frequency capacitive loop is overwhelmed by the capacitive characteristics associated with Mg^+ in the mediate frequency range. For example, when R_{Mg+} becomes much smaller than $R_{coating}$, and C_{Mg+} is significantly larger than $C_{s/m}$, then $(R_{coating}+R_t)C_{s/m}$ may have a value smaller that of $R_{Mg+}C_{Mg+}$. In this case, the equivalent circuit may yield an EIS spectrum with one apparent capacitive loop in the high and mediate frequency ranges and an inductive loop in the low frequency range (see Figure 14(d)). This type of EIS has been experimentally measured in this study (Figure 7 (b)).

In Figure 8, the apparently undamaged and significantly damaged areas of Anomag anodized AZ91D after 21 days of salt-spray exhibit the same EIS characteristics but

different diameters of loops. The similar EIS spectra further support the blocking effect of the anodized coating. The inductive loop measured from the apparently undamaged coating suggests that corrosion has already initiated in this area. This has been confirmed by carefully examining this area again after EIS measurement. In fact, a tiny pitting damage has already occurred in this area as pointed by the arrow in Figure 8(a). This damage was too small to be picked up by naked eye at the first look.

According to the measured EIS characteristics, similar invisible corrosion damage should have occurred in KSP anodized Mg after 0.5 hour immersion, while KSP anodized AZ91D and ZE41 have not been affected, because the EIS of the KSP anodized Mg has some inductive points at low frequencies, but KSP anodized AZ91D and ZE41 don't exhibit any inductive characteristics in its EIS (see Figure 6(a)). Why the anodized Mg is less corrosion-resistant than the anodized ZE41 and AZ91D will be explained later.

In this study, it is impractical to work out the values of all the equivalent components (Figure 13) through curve-fitting of EISs. The complicated combination of equivalent components makes the acquisition of these parameters from measured EISs difficult. For example, the $R_{coating}$ and R_t of an anodized coating are difficult to decompose. When coating is broken, parameters $C_{s/m}$ and C_{Mg+} cannot be separated from measured capacitance. Nevertheless, R_1 can be easily obtained from the overall capacitance diameter of a measured EIS. In theory, it is equal to ($R_{coating}$+R_t+R_{Mg+}), and to some extend reflects the overall resistance of an anodized Mg alloy against corrosion.

4.3. Influencing factors

(1) Solution

According to the proposed corrosion mechanism and coating model (Figure 12), an anodized Mg alloy in a NaCl solution should first experience Cl^- ingress. Only after the chloride concentration has reached a critical threshold in the coating through-pores, can the surface film of the substrate in the through-pores be further damaged, the film-free area be enlarged, the anodized coating be dissolved, and the anodic dissolution of the substrate be significantly accelerated. If the concentration of chloride is low, the ingress of chloride into coating will be slow, the breakdown of the film on the substrate in the through-pores will be delayed, and the corrosion of the substrate will not be dramatically accelerated. Figure 4 shows indirect evidence for the effect of chloride concentration on the anodic dissolution and breakdown of the film on the substrate in through-pores. When the NaCl concentration decreases, the passive current of unanodized ZE41 becomes lower and its pitting potential more positive. The unanodized ZE41 should have a porous surface film, which can to some extent simulate the area of the substrate ZE41exposed in the coating through-pores.

In this study, the electrochemical characteristics of ZE41 under passive and corrosion states appear to be more evidently different in a solution with a lower concentration of NaCl (see Figure 4). This can be explained. First, an anodized Mg alloy should have a critical chloride threshold concentration, below which the alloy is stable. This critical concentration for Mg cannot be higher than the level for steels, and must be much lower than 5 wt.%. If there are two anodized Mg specimens; one is more corrosion resistant than the other. The chloride critical threshold for the more resistant specimen should be higher than that for the less resistant one. When the concentration of chloride in a test solution is only slightly higher than the threshold of the more resistant one, but considerably higher than that of the less resistant one, the latter will be corroded quickly, whereas the former may still be uncorroded in this period. Therefore, these two anodized specimens in a corrosion test can be clearly separated in time domain. On the contrary, if the concentration of chloride in a test solution is much higher than the critical thresholds of these two specimens, then both of them will be corroded rapidly and the difference between them in corrosion incubation time may become negligible. Second, at a lower concentration of chloride, a passive electrode has a lower passive current density and more positive pitting potential, which can be clearly displayed on its polarization curve. However, in a solution containing concentrated chlorides, e.g., 5 wt.% NaCl, a Mg alloy may have a pitting potential more negative than its corrosion potential. Consequently, its passive region and pitting potential will be overwhelmed by the dramatically increasing anodic current density on its anodic polarization curve [68]. In this case, a difference in passive current density or pitting corrosion potential cannot be demonstrated on measured polarization curves.

During corrosion, solution pH value can gradually increase up to ~11 [**Error! Bookmark not defined.**,**Error! Bookmark not defined.**] due to the hydrogen evolution and $Mg(OH)_2$ saturation. The solution alkalization can easily occur particularly in surface film-free areas for an unanodized specimen or in coating through-pores for an anodized sample due to relatively fast dissolution of Mg there. The alkalization rate can vary randomly with time, depending on surface film integrity and coating porosity before the solution is saturated by $Mg(OH)_2$. If a test solution is saturated with $Mg(OH)_2$, then the dissolution of Mg will get into a steady stage immediately, yielding reproducible polarization curves. This could be the reason for the better polarization curve reproducibility of ZE41 in $Mg(OH)_2$ saturated 5 wt.% NaCl solution than in 5 wt.% NaCl (see Figure 3).

(2) Substrate

The corrosion performance of an anodized Mg alloy is to a great degree determined by the substrate alloy according to the corrosion model (Figure 12). $R_{coating}$ can be affected by Cl^- ingress, while R_t and R_{Mg+} depend on corrosion resistance of the substrate. After Cl^- penetrates into the coating and reaches the substrate in the coating through-pores, the corrosion resistance of the substrate is actually responsible for the corrosion performance of the anodized alloy. Therefore, a corrosion resistant Mg alloy after anodizing is usually more corrosion resistant than a less corrosion resistant Mg alloy with the same anodizing treatment. Mg is not as corrosion resistant as ZE41, while AZ91D is more corrosion

resistant than ZE41 (see Table 1). Thus, after KSP anodizing, the KSP anodized Mg, ZE41 and AZ91D follow the same ranking order of corrosion resistance as their unanodized counterparts (Figure 1).

4.4. Protection performance

According to the corrosion model (Figure 12), EIS equivalent (Figure 12) and coating effects proposed earlier, the number of coating through-pores is a critical parameter determining the corrosion performance of an anodized Mg alloy. Fewer through-pores mean that corrosive species penetrate more difficultly through the coating to attack the substrate in a smaller area that is less likely to have active defects, which also imply that the anodized coating has more evident retarding, blocking and passivating effects. The coating thickness can affect the number of the through-pores. A pore is more likely to penetrate though a thin coating, acting as a through-pore. A more porous coating may have more through-pores than a less porous one, and hence a less porous anodized coating could have better protection performance.

The important role of the through-pores in coating protection has been indirectly supported by a comparison in corrosion performance of anodized ZE41 before and after a sealing treatment using electroless E-coating [**Error! Bookmark not defined.**]. A sealed area of the anodized alloy was found to be much more corrosion resistant than an unsealed region. SEM examination revealed that the sealing treatment did not alter the basic characteristics (e.g. pore size and shape) of relatively large pores in the anodized

coating, but it modified the micro-features, such as particles and crevices, in the pores. The microstructure modification in coating pores could close off some through-pores, and thus enhance the retarding and blocking effects of the coating.

In this study, the KSP and Tagnite anodized ZE41 specimens were exposed to salt spray. The results (Figure 2) indicate that Tagnite coating is more corrosion resistant than KSP. This is understandable, as the Tagnite coating is thicker than KSP on ZE41 (see Figure 10). Moreover, the relatively high stability of the Tagnite coating may be another reason for its better corrosion resistance. Figure 11 (b) shows that corrosion damage has occurred in the substrate and undermining developed underneath the Tagnite coating, while the Tagnite coating over there has not been completely dissolved. The remaining Tagnite coating over the undermining area may to some degree retard the corrosion development in the substrate.

4.5. Coating evaluation

Since the corrosion of an anodized Mg alloy is an electrochemical process in coating through-pores, the corrosion performance of an anodized Mg alloy can be assessed or estimated through measuring some electrochemical parameters that characterize the processes associated with coating through-pores.

When an anodized Mg alloy is immersed in a 5 wt.% NaCl solution or exposed in the same concentration of salt spray, the chloride concentration in coating pores should be initially lower than 5 wt.% due to the coating retarding effect. Before the NaCl concentration reaches 5 wt.%, corrosion should have been triggered at the substrate active/defective points in a coating through-pore. Considering that the solution in coating pores can be rapidly saturated by $Mg(OH)_2$, the corrosion initiation of an anodized Mg alloy is actually a result of the substrate Mg alloy reacting with a $Mg(OH)_2$ saturated solution containing a low concentration of NaCl. Therefore, it is reasonable/acceptable to use a low concentration NaCl solution saturated with $Mg(OH)_2$ to simulate the coating pore solution in assessing the corrosion performance of anodized Mg alloys.

Table 2 shows that the ranking of anodized samples based on E_{pt} measurements does not match that of their corrosion morphologies (Figure 1 and Figure 2). This is not surprising, because E_{pt} in most cases only indicates the resistance of a coating to breakdown damage at a potential significantly more positive than the corrosion potential; it does not characterize the corrosion around the corrosion potential which is more closely associated with the damage under immersion or spray condition. E_{corr} in theory cannot be directly related to corrosion rate. It is affected by too many material and environment factors. Even though the values of E_{corr} listed in Table 2 accidentally correspond well to the corrosion morphologies (Figure 1 and Figure 2), it is groundless to use E_{corr} as a parameter to indicate the corrosion performance of anodized Mg alloys.

The parameters in Table 2 correlated best with the corrosion morphologies (Figure 1) of KSP anodized alloys under immersion conditions are R_1 and I_p. They can be ranked in the following orders:

R_1: AZ91D > ZE41 > Mg
I_p: AZ91D < ZE41 < Mg

These two parameters are closely associated with corrosion rate. I_p is equivalent to the anodic dissolution rate of the substrate in coating through-pores according to the corrosion model (Figure 12). It is determined by the stability (R_t+R_{Mg+}) of the substrate exposed in the coating through-pores and the resistance ($R_{coating}$) of the through-pores. There is R_1=$R_{coating}$+R_t+R_{Mg+} according to the equivalent circuit (Figure 13). It characterizes the overall resistance of the electrochemical processes involved in the corrosion at the coating/substrate interface in coating through-pores. Therefore, I_p and R_1 represent the overall electrochemical rate and resistance of the coating through-pores, respectively. The coincidence between the ranking order of the immersion corrosion morphologies (Figure 1) and the values of I_p and R_1 (Table 2) suggests that R_1 and I_p can reasonably reflect the coating protection performance of anodized Mg alloys. This assertion has been further confirmed by the salt spray corrosion morphologies (Figure 2); the degrees of corrosion damage correspond well to the ranking orders of R_1 and I_p for KSP and Tagnite anodized ZE41 (Table 2).

In theory, EIS measurement at corrosion potential cannot change the status of an electrode system or cause damage to a steady corroding system. However, in practice the corrosion potential of an anodized Mg alloy may drift away from its initial value that is normally set as a fixed potential during EIS measurement under potentiostatic mode. While a constant potential is applied to this system, the drift of the corrosion potential of a corrosion system is equivalent to that the corrosion system is polarized by a potential difference. If the difference is large enough, it may alter the status of the corrosion system and result in corrosion damage. Fortunately, anodized Mg alloys are more stable than bare Mg alloys, and EIS measurements can usually be finished in about 2 hours. The potential drift is actually not very evident during EIS test. In this case, the possible damage caused by potential drift should not be a big concern. In future, this problem may be solved if EIS is performed under galvanostatic mode with a carefully selected amplitude of AC current perturbation.

Since EIS measurement does not evidently affect a measured corrosion system while polarization curve technique is destructive to a specimen, measuring R_1 through EIS should be a suitable method for corrosion monitoring of anodized Mg alloys. Apart from the quantitative parameter R_1, the corrosion of an anodized Mg alloy can also be indicated by EIS inductive characteristics, which is more sensitive than naked eye observation. The emerging of inductive characteristics is important information when EIS is employed as a non-destructive method for assessing or monitoring the corrosion of anodized Mg alloys.

5. Conclusions

1. An anodized coating can effectively inhibit the corrosion of Mg alloys, through blocking most the substrate surface area, retarding the ingress of corrosive solution, and passivating the substrate defective/active points. The through-pore in the anodized coating is the most critical defect that determines the coating protection performance. Coating thickness have an influence on the number of through-pores, and thus affect the corrosion resistance of an anodized Mg alloys.

2. The corrosion of an anodized Mg alloy initiates under a through-pore of the anodized coating. It follows the same mechanism as that of the substrate alloy, but all the electrochemical corrosion reactions are restricted in the through-pore. The dissolution of Mg at the substrate/coating interface in the through-pores determines the corrosion resistance of the anodized coating. Therefore, the corrosion performance of an anodized Mg alloy also depends on the corrosion resistance of the substrate alloy.

3. The passive current density measured from the polarization curve and the overall capacitive resistance obtained from the EIS spectrum of an anodized Mg alloy can reasonably indicate the corrosion resistance of this anodized specimen. Corrosion initiation of the anodized system can be sensitively detected based on the emerging inductive characteristics in EIS.

Acknowledgements

Authors gratefully acknowledge the technical support from the Australia Microscopy & Microanalysis Research Facility at the Centre for Microscopy and Microanalysis, the University of Queensland.

References

[1] C.L.Makar and J.Kruger, Corrosion of Magnesium, International Materials Reviews 38 (1993) 138 -153.
[2] G.-L. Song (ed.), Corrosion of Magnesium Alloys, Woodhead Publishing Limited, UK, 2011.
[3] G.-L. Song (ed.), Corrosion Prevention of Magnesium Alloys, Woodhead Publishing Limited, UK, 2013.
[4] F.Witte, J.Fischer, J.Nellesen, C.Vogt, J.Vogt, T.Donath, F.Beckmann, In vivo corrosion and corrosion protection of magnesium alloy LAE442, Acta Biomaterialia 6 (2010) 1792-1799.
[5] M.P.Staiger, A.M.Pietak, J.Huadmai, G.Dias, Magnesium and its alloys as orthopedic biomaterials: A review, Biomaterials 27 (2006) 1728-1734.
[6] R.Rettig, S.Virtanen, Composition of corrosion layers on a magnesium rare-earth alloy in simulated body fluids, Journal of Biomedical Materials Research 88 (2009) A 359–369.
[7] G.Song, S. Song, Corrosion Behaviour of Pure Magnesium in a Simulated Body Fluid, Acta Physico Chimica Sinica 22 (2006) 1222-1226.
[8] G.Cole, Issues that Influence Magnesium's Use in the Automotive Industry, Materials Science Forum 419-422 (2003) 43-50.
[9] ASM Handbook, Vol 13, Corrosion, ASM International, Fourth Printing 1992.
[10] G.-L. Song, Z. Xu, Effect of Microstructure Evolution on Corrosion of Different Crystal Surfaces of AZ31 Mg alloy in a Chloride Containing Solution, Corrosion Science 54 (2012) 97-105.
[11] G.-L. Song, Z. Xu, The surface, microstructure and corrosion of magnesium alloy AZ31 sheet, Electrochimica Acta 55 (2010) 4148-4161.
[12] G.-L. Song, Effect of tin modification on corrosion of AM70 magnesium alloy, Corrosion Science 51 (2009) 2063-2070.
[13] E.Aghion and B.Bronfin, Magnesium Alloys Development towards the 21st Century, Matrerials Science Forum 350-351 (2000) 19-30.
[14] G.-L. Song, M. Liu, “The Effect of Mg Alloy Substrate on “Electroless” E-Coating Performance”, Corrosion Science, 53 (2011) 3500-3508
[15] G.-L. Song, Effect of Texture on the Corrosion Behavior of AZ31 Mg Alloy, JOM 64 (2012) 671 -679.
[16] C.Blawert, W.Dietzel, E.Ghali, G.Song, Anodizing treatments for magnesium alloys and their effect on corrosion resistance in various environments---a critical review, Advanced Engineering Materials 8 (2006) 511-533.
[17] D.E.Bartak, B.E.Lemieux, E.R.Woolsey, Two-step chemical/electrochemical process for coating magnesium alloys, US patent 5240589 A, Aug 31, 1993

[18] Thomas Francis Barton, John Arnold Macculloch, Philip Nicholas Ross, Anodization of magnesium and magnesium based alloys, US 6280598 B1, Aug. 28,2001
[19] E.L. Schmeling, B. Roschenbleck, M. H. Weidemann, Method of producing protective coatings that are resistant to corrosion and wear on magnesium and magnesium alloys, US Patent 4 978 432, December 18,1990.
[20] A.S.Shatrov, Method for producing hard protection coatings on articles made of aluminium alloys, WO 1999031303 A8, May 25, 2001
[21] H.A.Evangelides, Magnesium and protective coatings for Magnesium, Plating 45 (1958) 493-498.
[22] DOW MAGNESIUM, Operation in Magnesium Finishing, The Dow Chemical Company, 1990
[23] Y.Choi, S.Salman, K.Kuroda, M.Okido, Improvement in corrosion characteristics of AZ31 Mg alloy by square pulse anodizing between transpassive and active regions, Corrosion Science 63 (2012) 5-11.
[24] L.Chai, X.Yu, Z.Yang, Y.Wang, M.Okido, Anodizing of magnesium alloy AZ31 in alkaline solutions with silicate under continuous sparking , Corrosion Science 50 (2008) 3274-3279.
[25] S.Moon, Y.Nam, Anodic oxidation of Mg–Sn alloys in alkaline solutions , Corrosion Science 65 (2012) 494 -501.
[26] D.Veys-Renaux, E.Rocca, G.Henrion, D.Veys-Renaux, E.Rocca, G.Henrion, Electrochemistry Communications 31 (2013)42-45.
[27] M.Santamaria, F.Quarto, S.Zanna, P.Marcus, The influence of surface treatment on the anodizing of magnesium in alkaline solution, Electrochimica Acta 56 (2011) 10533-10542.
[28] Y.Choi, S.Salman, K.Kuroda, M.Okido, Synergistic corrosion protection for AZ31 Mg alloy by anodizing and stannate post-sealing treatments, Electrochimica Acta 97 (2013) 313-319.
[29] D.Ivanou, M.Starykevich, A.Lisenkov, M.Zheludkevich, H.Xue, S.Lamaka, M.Ferreira, Plasma anodized ZE41 magnesium alloy sealed with hybrid epoxy-silane coating , Corrosion Science 73 (2013) 300-308.
[30] S.Moon, Y.Nam, C.Yang, Y.Jeong, Growth of anodic oxide films on AC2A alloy in sulphuric acid solution , Corrosion Science 53 (2011) 1547-1553.
[31] X.Fan, Y.Wang, B.Zou, L.Gu, W.Huang, X.Gao, Preparation and corrosion resistance of MAO/Ni–P composite coat on Mg alloy, Applied Surface Science 277 (2013) 272-280.
[32] G. Song, Electroless E-coating ---An Innovative Surface Treatment for Magnesium Alloys, Electrochemical and Solid-State Letters 12 (2009) D77-D79.
[33] G.-L. Song, Electroless deposition of pre-film of electrophoresis coating and its corrosion resistance on a Mg alloy, Electrochimica Acta 55 (2010) 2258-2268.
[34] G.-L. Song, M. Liu, , The Effect of Surface Pretreatment on the Corrosion Performance of Electroless E-Coating Coated AZ31, Corrosion Science 62 (2012) 61-72.
[35] G. Song, An irreversible dipping sealing technique for anodized ZE41 Mg alloy, Surface & Coatings Technology 203 (2009) 3618 -3625.

[36] G.-L. Song, A dipping E-coating for Mg alloys, Progress in Organic coatings 70 (2011) 252 -258.
[37] S.Song, W. Shen, M. Liu, G.-L. Song, Corrosion Study of New Surface Treatment/Coating for AZ31B Magnesium Alloy, Surface Engineering 28 (2012) 486-490.
[38] Z.Shi, G.Song, A.Atrens, Influence of anodizing current on the corrosion resistance of anodized AZ91D magnesium alloy, Corrosion Science 48 (2006) 1939-1959.
[39] Z.Shi, G.Song, A.Atrens, Corrosion resistance of anodized single-phase Mg alloy, Surface & Coatings Technology 201 (2006) 492-503.
[40] R.F.Zhang, Film formation in the second step of micro-arc oxidation on magnesium alloys, Corrosion Science 52 (2010) 1285-1290.
[41] M.Saenz de Miera, M.Curioni, P.Skeldon, G.E.Thompson, The behaviour of second phase particles during anodizing of aluminium alloys, Corrosion Science 52 (2010) 2489-2497.
[42] T.Lim, H.Ryu, S.Hong, Electrochemical corrosion properties of CeO2-containing coatings on AZ31 magnesium alloys prepared by plasma electrolytic oxidation, Corrosion Science 62 (2012) 104 -111.
[43] T.Lei, C.Ouyang, W.Tang, L.Li, L.Zhou, Enhanced corrosion protection of MgO coatings on magnesium alloy deposited by an anodic electrodeposition process, Corrosion Science 52 (2010) 3504 -3508.
[44] L.Liu, P.Yang, C.Su, H.Guo, M.An, Microstructure and Corrosion Behavior of Micro-Arc Oxidation Film on Magnesium Alloy, International Journal of Electrochemical Science 8 (2013) 6077-6084.
[45] Z.Shi, G.Song, A.Atrens, Corrosion performance of anodized magnesium alloy, Corrosion Science 48 (2006) 3531-3546.
[46] ASTM B117, Standard practice for operating salt spray (fog) apparatus, ASTM International, 2009.
[47] X. Liu, T. Zhang, Y. Shao, G.Meng, F. Wang, Effect of alternating voltage treatment on the corrosion resistance of pure magnesium, Corrosion Science 51 (2009) 1772-1779.
[48] J. Chen, J.Wang, E. Han, J.Dong, W.Ke, AC impedance spectroscopy study of the corrosion behavior of an AZ91 magnesium alloy in 0.1 M sodium sulfate solution, Electrochimica Acta 52 (2007) 3299-3309.
[49] M. Mosiałek, G. Mordarski, P. Nowak, W. Simka, G.Nawrat, M. Hanke,R.P. Socha, J. Michalska, Phosphate–permanganate conversion coatings on the AZ81 magnesium alloy: SEM, EIS and XPS studies, Surface and Coatings Technology 206 (2011) 51-62.
[50] F. Zucchi, A. Frignani, V. Grassi, G. Trabanelli, C. Monticelli, Stannate and permanganate conversion coatings on AZ31 magnesium alloy, Corrosion Science 49 (2007) 4542-4552.
[51] M. Chen, N.Cheng, Y.Ou, J. Li, Corrosion performance of electroless Ni–P on polymer coating of MAO coated AZ31 magnesium alloy, Surface and Coatings Technology 232 (2013) 726-733.
[52] R. Arrabal, J.M. Mota, A. Criado, A. Pardo, M. Mohedano, E. Matykina , Assessment of duplex coating combining plasma electrolytic oxidation and

polymer layer on AZ31 magnesium alloy, Surface and Coatings Technology 206 (2012) 4692-4703.

[53] G. Liu, S. Tang, D. Li, J. Hu, Self-adjustment of calcium phosphate coating on micro-arc oxidized magnesium and its influence on the corrosion behaviour in simulated body fluids, Corrosion Science 79 (2014) 206-214.

[54] Y. Gu, C. Chen, S. Bandopadhyay, C. Ning, Y. Zhang, Y. Guo, Corrosion mechanism and model of pulsed DC microarc oxidation treated AZ31 alloy in simulated body fluid, Applied Surface Science 258 (2012) 6116-6126.

[55] D.K. Ivanou, M. Starykevich, A.D. Lisenkov, M.L. Zheludkevich, H.B. Xue, S.V. Lamaka, M.G.S. Ferreira, Plasma anodized ZE41 magnesium alloy sealed with hybrid epoxy-silane coating, Corrosion Science 73 (2013) 300-308.

[56] J. Liang, P. Bala Srinivasan, C. Blawert, W. Dietzel, Influence of pH on the deterioration of plasma electrolytic oxidation coated AM50 magnesium alloy in NaCl solutions, Corrosion Science 52 (2010) 540-547.

[57] H. Ardelean, I. Frateur, S. Zanna, A. Atrens, P. Marcus, Corrosion protection of AZ91 magnesium alloy by anodizing in niobium and zirconium-containing electrolytes, Corrosion Science 51 (2009) 3030-3038.

[58] S.Yagi, A.Sengoku, K.Kubota, E. Matsubara, Surface modification of ACM522 magnesium alloy by plasma electrolytic oxidation in phosphate electrolyte, Corrosion Science 57 (2012) 74-80.

[59] G.Wu, X.Zhang, Y.Zhao, J.M.Ibrahim, G.Yuan, P.Chu, Plasma modified Mg-Nd-Zn-Zr alloy with enhanced surface corrosion resistance, Corrosion Science 78 (2014) 121-129.

[60] X.Guo, M.An, Experimental study of electrochemical corrosion behavior of bilayer on AZ31B Mg alloy, Corrosion Science 52 (2010) 4017-4027.

[61] T.S.Lim, H.S.Ryu, S.-H. Hong, Electrochemical corrosion properties of CeO_2-containing coatings on AZ31 magnesium alloys prepared by plasma electrolytic oxidation, Corrosion Science 62 (2012) 104-111.

[62] F. Cao, Z. Shi, G.-L. Song, M. Liu, A. Atrens, Corrosion behaviour in salt spray and in 3.5 % NaCl solution saturated with $Mg(OH)_2$ of as-cast and solution heat-treated binary Mg-X alloys: X = Mn, Sn, Ca, Zn, Al, Zr, Si, Sr, Corrosion Science 76 (2013) 60-97.

[63] Z. Shi, F. Cao, G.-L. Song, M. Liu, A. Atrens, Corrosion behaviour in salt spray and in 3.5 % NaCl solution saturated with $Mg(OH)_2$ of as-cast and solution heat-treated binary Mg-RE alloys: RE = Ce, La, Nd, Y, Gd, Corrosion Science 76 (2013) 98-118.

[64] F. Cao, Z. Shi, J. Hofstetter, P. J Uggowitzer, G. Song, M. Liu, A. Atrens, "Corrosion of ultra-high-purity Mg in 3.5% NaCl solution saturated with $Mg(OH)_2$, Corrosion Science 75 (2013) 78-99.

[65] Z.Shi, G.Song, A.Atrens, Influence of the β phase on the corrossion performance of anodised coatings on magnesium-aluminium alloys, Corrosion Science 47 (2005) 2760-2777.

[66] G.Song, A.Atrens, D.StJoh, X.Wu, J.Nairn, Anodic Dissolution of Magnesium in Chloride and Sulphate Solutions, Corrosion Science 39 (1997) 198 -2004.

[67] G.Song, A.Bowles, D.StJohn, Corrosion resistance of aged die cast magnesium alloy AZ91D, Materials Science & Engineering-A 366 (2004) 74-86.

[68] G.Song, A.Atrens, Understanding Magnesium Corrosion, a Framework for Improved Alloy Performance, Advanced Engineering Materials 5 (2003) 837-858.

Figure captions

Figure 1. Corrosion morphologies of anodized specimens after immersion in 5 wt.% NaCl solution: (a) KSP anodized Mg after 1 day immersion; (b) KSP anodized AZ91D after 11day immersion; (c) KSP anodized ZE41 after 2 day immersion.

Figure 2. Corrosion morphologies of anodized ZE41 after exposure in 5 wt.% NaCl salt spray: (a) KSP anodized then exposed for 3 days; (b) Tagnite anodized then exposed for 12 days

Figure 3. Repeatedly measured polarization curves for ZE41 in (a) 5 wt.% NaCl solution and (b) $Mg(OH)_2$ saturated 5 wt.% NaCl solution

Figure 4. Typical anodic polarization curves for ZE41 and KSP anodized ZE41 in $Mg(OH)_2$ saturated NaCl solutions.

Figure 5. Typical anodic polarization curves for KSP anodized Mg, ZE41 and AZ91D, and Tagnite anodized ZE41 in $Mg(OH)_2$ saturated 0.1 wt. % NaCl solution.

Figure 6. Typical AC electrochemical impedance spectra for (a) unanodized ZE41, (b) KSP anodized Mg, (c) KSP anodized ZE41 and (d) KSP anodized AZ91D after immersion in $Mg(OH)_2$ saturated 0.1 wt.% NaCl solution for 0.5 hour.

Figure 7. EIS evolution with immersion time for anodized ZE41 in $Mg(OH)_2$ saturated 0.1 wt.% NaCl solution: (a) KSP anodizing, (b) Tagnite anodizing

Figure 8. Typical AC electrochemical impedance spectra obtained from the circled areas of Anomag anodized AZ91D specimens that had been exposed in 5 wt.% NaCl salt spray for 21 days: (a) the area where corrosion damage cannot be visualized by naked eye, (b) the significantly corroded area.

Figure 9. Topographic SEM images of KSP coatings on (a) Mg, (b) AZ91D and (c) ZE41, and (d) Tagnite coating and (e) Anomag coating on ZE41

Figure 10. Cross-sectional SEM images of (a) KSP, (b) Tagnite and (c) Anomag anodized ZE41.

Figure 11. (a) Cross-sectional optical photo of an uncorroded area of Anomag anodized ZE41 after immersion in $Mg(OH)_2$ saturated 0.1 wt.% NaCl for 20 hours, and (b) cross-sectional SEM image of a corroded area of Tagnite anodized ZE41 after 12 days of exposure in 5 wt.% NaCl salt spray.

Figure 12. Schematic illustration of the corrosion of an anodized Mg alloy

Figure 13. Equivalent circuit for an anodized Mg alloy

Figure 14. Calculated EISs according to the equivalent circuit shown in Figure 13: (a) unanodized Mg; (b) a thick anodized coating (value "10^{20}" is used to stand for ∞ in calculation); (c) an anodized coating penetrated by of corrosive solution before corrosion initiation; (d) surface film and coating damaged by corrosive solution. For universality, all the parameter values used in calculation have no units.

Figures

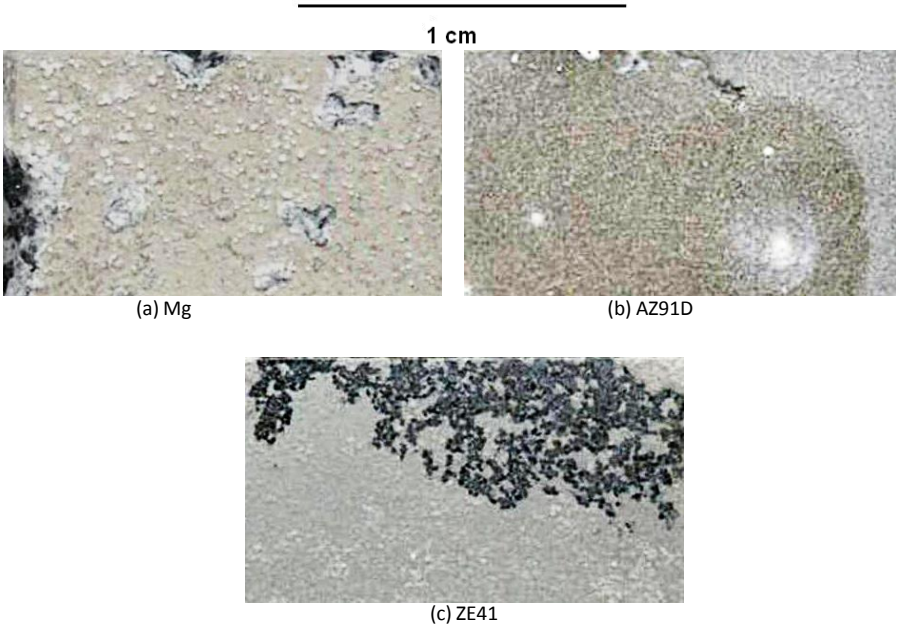

Figure 1. Corrosion morphologies of anodized Mg and its alloys after immersed in 5wt% NaCl solution: (a) KSP anodized Mg after 1 day immersion; (b) KSP anodized AZ91D after 11day immersion; (c) KSP anodized ZE41 after 2 day immersion.

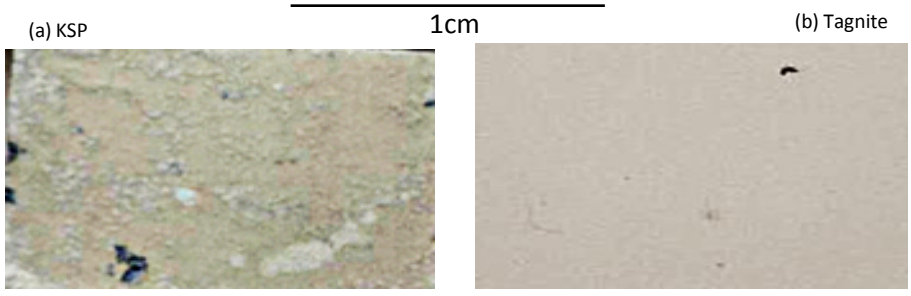

Fig.2. Corrosion morphologies of anodized ZE41 after exposure in 5wt% NaCl salt spray: (a) KSP anodized then exposed for 3 days; (b) Tagnite anodized then exposed for 12 days

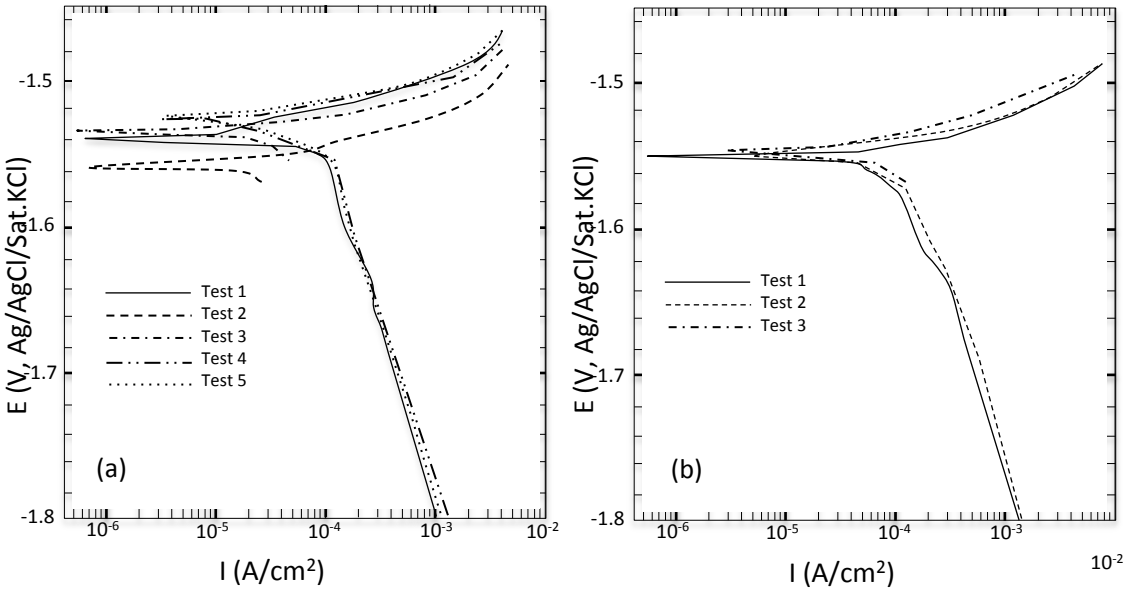

Figure 3. Repeatedly measured polarisation curves for ZE41 in (a) 5wt% NaCl solution and (b) $Mg(OH)_2$ saturated 5wt.% NaCl solution

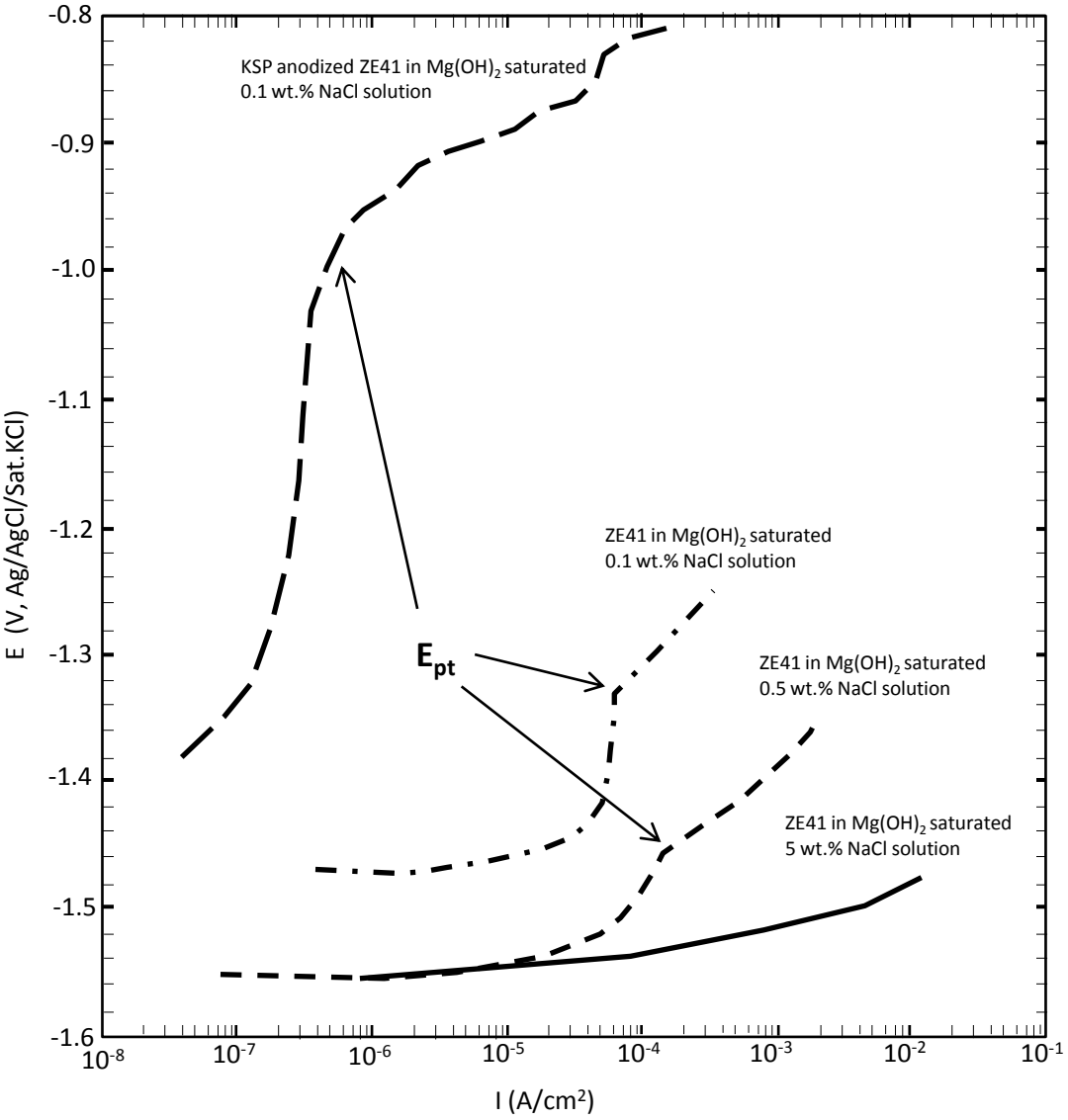

Figure 4. Typical anodic polarisation curves for ZE41 and KSP anodized ZE41 in $Mg(OH)_2$ saturated NaCl solutions.

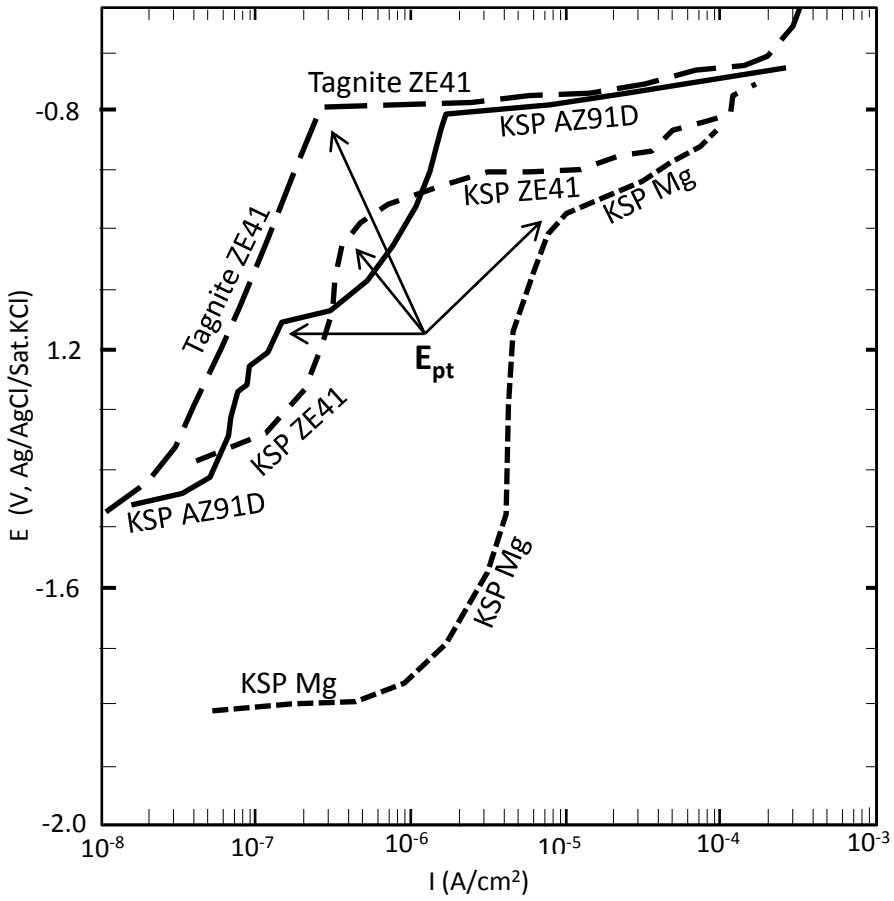

Figure 5. Typical anodic polarisation curves for KSP anodised Mg, ZE41 and AZ91D and Tagnite anodized ZE41 in $Mg(OH)_2$ saturated 0.1 wt. % NaCl solution

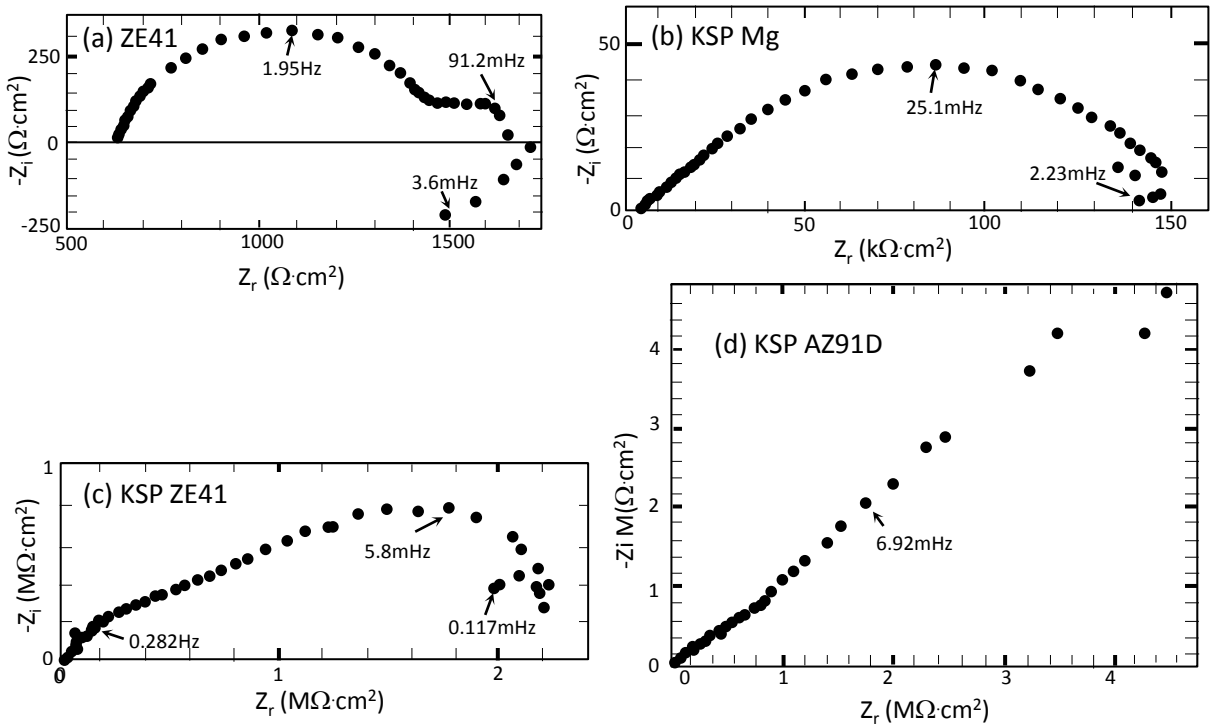

Figure 6. Typical AC electrochemical impedance spectra for (a) unanodized ZE41, (b) KSP anodized Mg, (c) KSP anodized ZE41 and (d) KSP anodized AZ91D after immersion in $Mg(OH)_2$ saturated 0.1 wt.% NaCl solution for 0.5 hour.

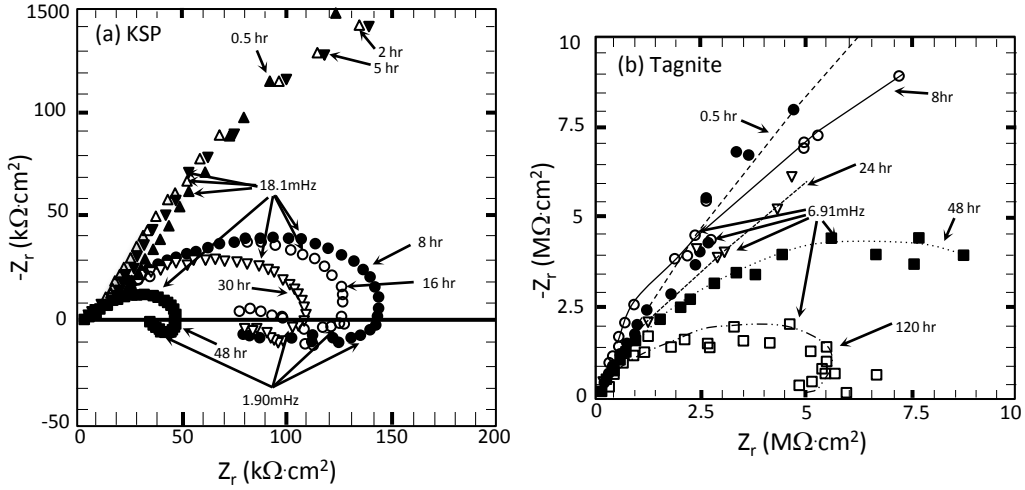

Fig.7. EIS evolution with immersion time for anodized ZE41 in $Mg(OH)_2$ saturated 0.1wt% NaCl solution: (a) KSP anodizing, (b) Tagnite anodizing

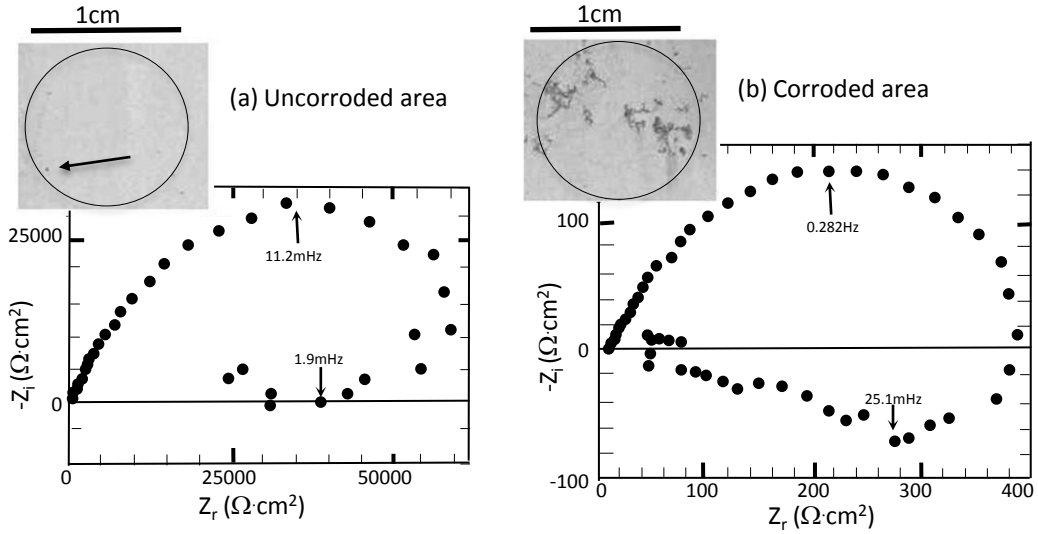

Figure 8. Typical AC electrochemical impedance spectra obtained from the circled areas of Anomag anodized AZ91D specimens that had been exposed in 5wt.% NaCl salt spray for 21 days: (a) the area where corrosion damage cannot be visualised by naked eye, (b) the significantly corroded area.

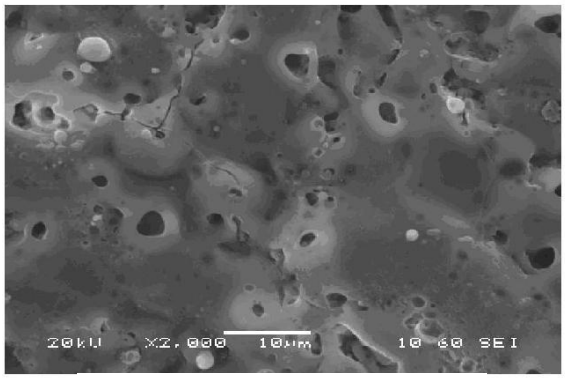

(a) KSP Mg; pore size ~ 1.73µm, Std.dev.=0.77µm

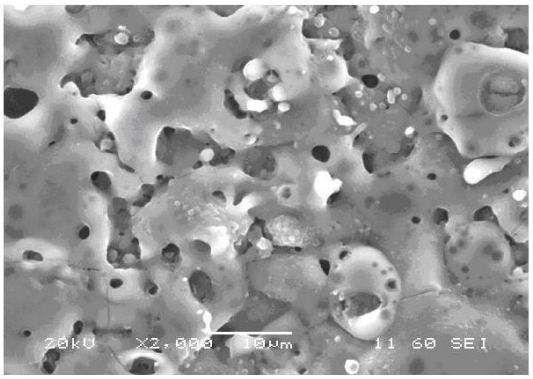

(b) KSP AZ91D; pore size ~1.37µm, Std.dev.=1.22µm

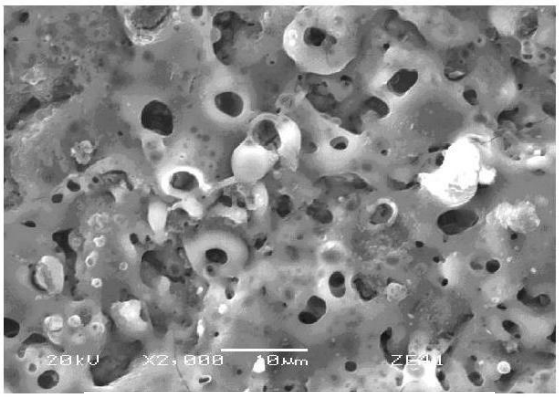

(c) KSP ZE41; pore size ~1.53µm, Std.dev.=0.92µm

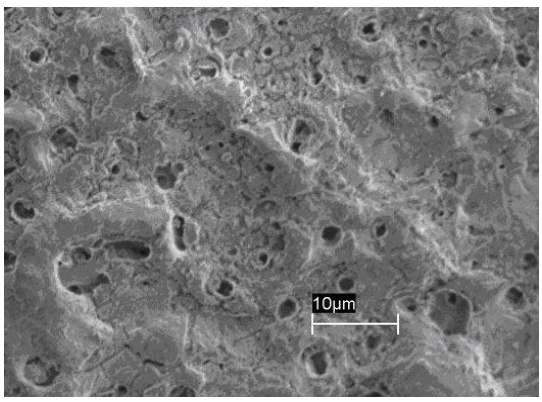

(d) Tagnite ZE41; pore size~1.41µm, Std.dev.=1.09µm

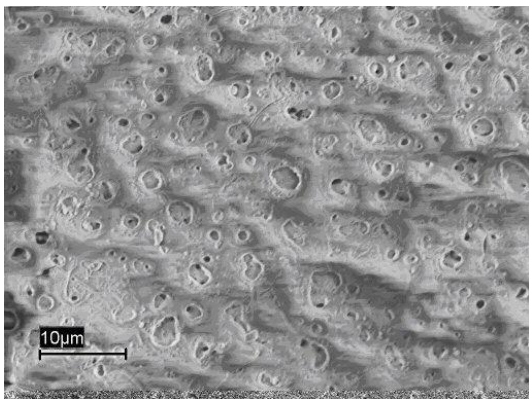

(e) Anomag ZE41; pore size~0.75µm, Std.dev.=0.25µm

Figure 9. Topographic SEM images of KSP coatings on (a) Mg, (b) AZ91D and (c) ZE41, and (d) Tagnite coating and (e) Anomag coating on ZE41

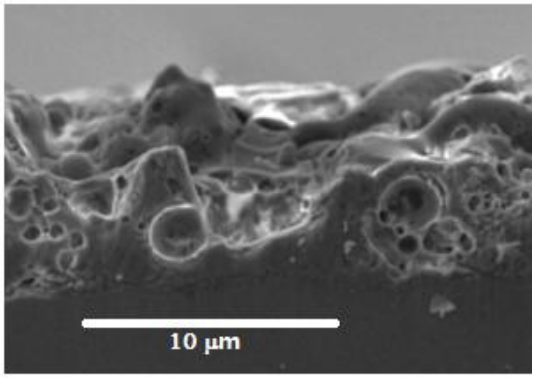

(a) KSP ZE41; pore size ~ 1.57µm, Std.dev.=10.85µm

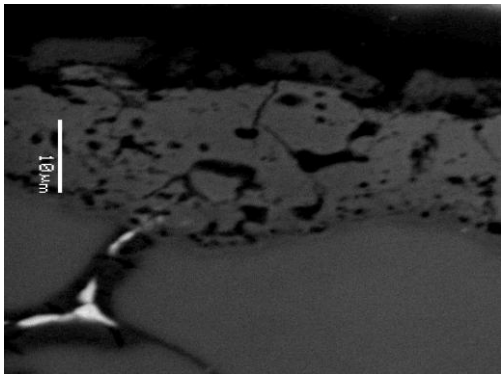

(b) Tagnite ZE41; pore size ~1.77µm, Std.dev.=1.31µm

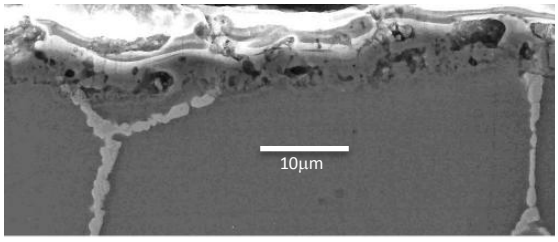

(c) Anomag ZE41, pore size ~ 1.95µm, Std.dev.=1.44µm

Figure 10. Cross-sectional SEM images of (a) KSP, (b) Tagnite and (c) Anomag anodized ZE41.

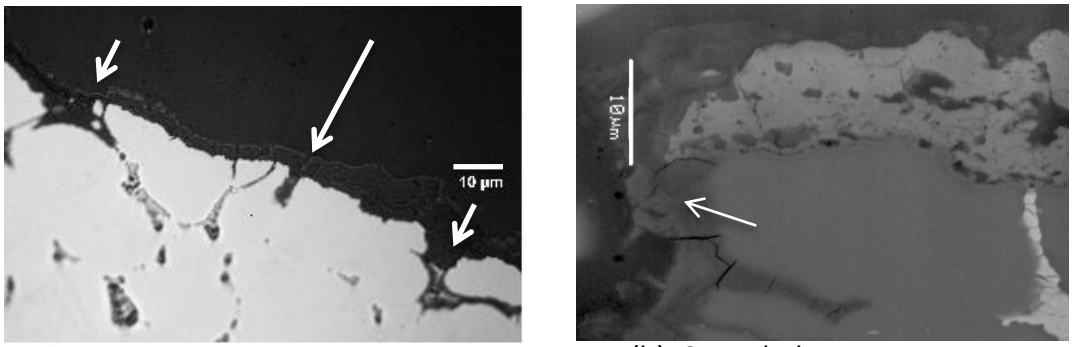

(a) Uncorroded area (b) Corroded area

Figure 11. (a) Cross-sectional optical photo of a selected apparently uncorroded area of Anomag anodized ZE41 after immersion in $Mg(OH)_2$ saturated 0.1 wt.% NaCl for 20 hours, and (b) cross-sectional SEM image of a corroded area of Tagnite anodized ZE41 after 12 days of exposure in 5wt.% NaCl salt spray.

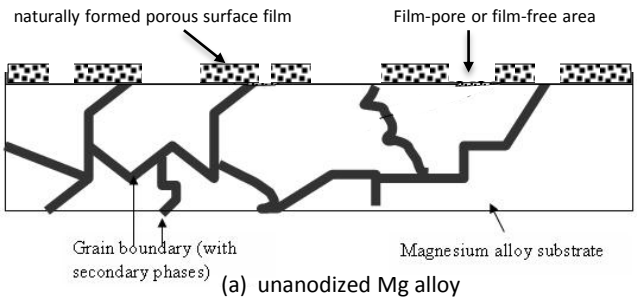

(a) unanodized Mg alloy

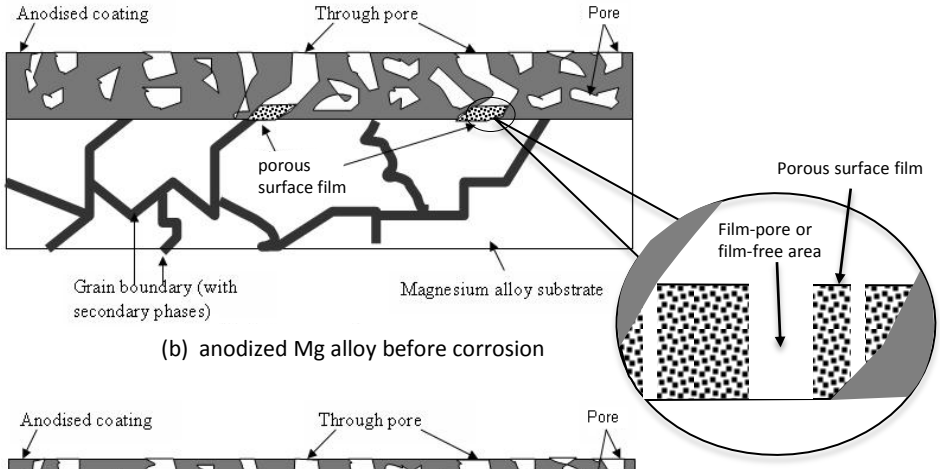

(b) anodized Mg alloy before corrosion

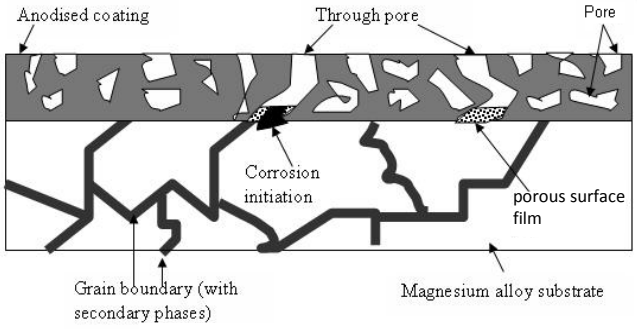

(c) corrosion initiation in anodized Mg alloy

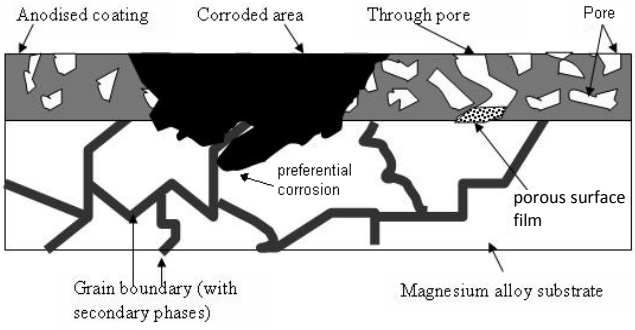

(d) corrosion damage of anodized Mg alloy

Figure 12. Schematic illustration of the corrosion of an anodised magnesium alloy

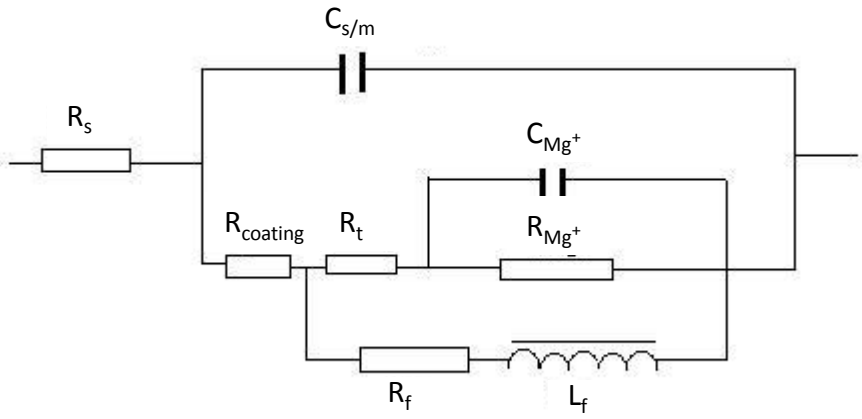

Figure 13. Equivalent circuit for an anodised Mg alloy

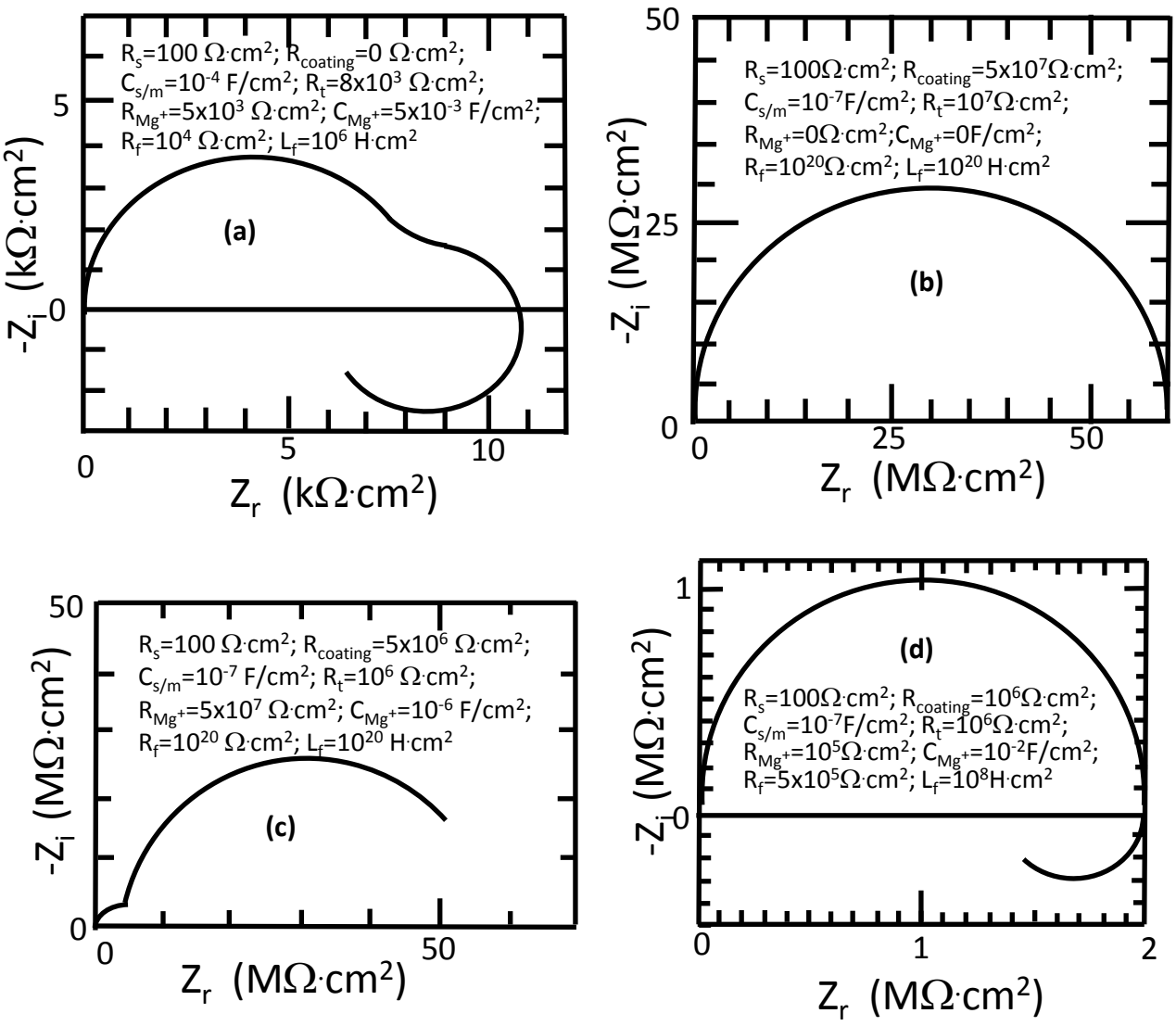

Figure 14. Calculated EISs according to the equivalent circuit shown in Figure 14: (a) unanodized Mg; (b) a thick anodized coating (value "10^{20}" is used to stand for ∞ in calculation); (c) an anodized coating penetrated by of corrosive solution before corrosion initiation; (d) surface film and coating damaged by corrosive solution. For universality, the parameter values used in calculation have no units.

Highlights

- The number of through-pores in the coating determines the anodized Mg corrosivity
- The Mg dissolution in the through-pores is a time dependent multi-reaction process
- A more stable substrate alloy has a lower Mg dissolution rate in the through-pores